Design of the feed system of a hybrid rocket engine

M. Demoly[a], J. Fissette[a], O. Vielpeau[a], A. Treilhes[a], N. Rizzo[a], J. Rèbre[a], J. Mulpas[a], V. Jacaranda-Lakiss-Marques[a], E. Jean-Bart[a,b], R. Mercier[a,b], B. Fiorina[a,b], O. Gicquel[a,b]
[a]Ecole Centrale Paris
Grande Voie des Vignes, 92290 Châtenay-Malabry, France
[b] CNRS, UPR 288, Laboratoire d'Energétique Moléculaire et Macroscopique, Combustion (EM2C)
Grande Voie des Vignes, 92290 Châtenay-Malabry, France

Abstract

Hybrid Rocket Engine (HRE) is a promising propulsion technology for nanosatellite launchers and civil suborbital flights. Nevertheless, a global optimization of the HRE subsystems has to be conducted to ensure safety and reliability. This first year engineering students contribution presents a design strategy for both an oxidizer tank and an HRE injection system. Conception and realization of both parts are first detailed. Two dedicated test benches are then presented and main results of the experimental campaigns are analyzed.

1. Introduction

Over the last decade, space industry has experienced a radical change with the apparition of private companies providing low-cost solutions for nanosatellites launch and civil suborbital flights. In this context, Hybrid Rocket Engine (HRE) technology seems to meet safety and cost-efficiency requirements compared to widely used solid and liquid propulsion systems. From a general point of view, the design of such engine is not straightforward because of its intrinsic transient behavior, i.e., combustion chamber geometry continuously varies with the operating time [1]. In addition, combustion process can be highly unstable because of the potential coupling of turbulent multiphase reacting flow and acoustic modes of the chamber [2]. In practice, such interactions may result in low-frequency instabilities, damage the payload and lead to a partial destruction of the HRE. Control of oxidizer injection, optimization of atomization process and chamber aerodynamics are then compulsory to ensure a stable behavior of the diffusion flame and improve combustion efficiency [3]. Hence, HRE reliability and performance are closely linked to injection and feed systems. This contribution first proposes a concrete and operational solution to limit oxidizer sloshing and then ensure a continuous feeding of the combustion chamber during a flight. Design, realization and experimental characterization of the anti-sloshing system are detailed. In a second part, a new injector geometry adapted to both single and multi-port fuel grains is presented and experimentally characterized.

2. Limiting oxidizer sloshing in hybrid rocket engines

The conception of the present anti-sloshing system, based on the identification of the sloshing modes [4] during a typical rocket flight, is first described. A combination of several simple anti-sloshing systems [5] has been designed to prevent the identified modes to appear. Finally, a test campaign has been conducted to assess the efficiency of the proposed detachable anti-sloshing system.

2.1 Investigated anti-sloshing device

During a flight, the vibrations of the engine can induce a sloshing of the propellant, which produces a random load on the structure and can alter the continuous supply of the engine, the trajectory of the rocket or the thermodynamic conditions of the propellant, here liquid N_2O. According to Royon-Lebeaud [4], three main sloshing modes are observable in a cylindrical tank:

1. An anti-symmetric mode during which the liquid rises against the walls of the tank.

2. A rotating mode causing a rotation of the liquid within the tank. It appears for greater excitation frequencies than the anti-symmetric mode.
3. A chaotic mode during which the waves unstick from the walls. It creates unpredictable liquid-gas interface movements.

The three identified modes can be encountered in a practical situation and they all have to be damped by the selected anti-sloshing device. Many existing devices can be found in the literature and can be sorted under different categories as proposed in [5]:

- Rings. They can reduce the anti-symmetric and the chaotic modes, for a large range of filling level. However, rings do not protect from the rotating mode. They are easy to build but difficult to integrate within the tank.
- Domes. A dome is a hemispherical device that is placed on the top of the tank. It can reduce both the anti-symmetric and the chaotic modes if the filling level is high enough but becomes useless for low filling levels. Domes do not prevent from the rotating mode.
- Bladders. Bladders are membranes filling the tank as it empties. They completely stop the anti-symmetric and the chaotic modes because no empty space is left to the liquid. Bladders also do not prevent from the rotating mode.
- Honeycomb. Honeycomb consists in a partitioning of the tank in small cubic volumes. It affects all the modes and seems to be the most effective device, but it is extremely hard to build and increases significantly the weight of the tank.

In this study, it is proposed to combine several simple anti-sloshing systems in order to ensure an action on all the sloshing modes to prevent. For that purpose, a device composed of two plates disposed along the height of the tank was built. A series of rings has been associated to both plates. The rings are disposed close enough from each other to damp the antisymmetric or the chaotic mode while the plates prevent from the rotating mode. Circular arcs were drilled in each ring to reduce propellant retention as shown in Fig. 1b. A 3-D view of the anti-sloshing device is shown in Figure 1a. The final device is very light and its mass is 350 g for a $5 \cdot 10^{-3}$ m^3 tank representing only 7% of the total mass of the filled tank. In order to perform the different experiments with a constant mass of sloshing liquid, the experiments made without the anti-sloshing device were conducted with an additional 110 g mass of water.

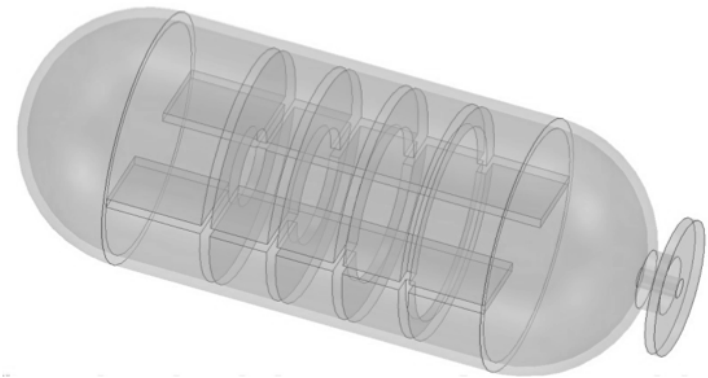

(a) 3-D view of the anti-sloshing device integrated in an oxidizer tank.

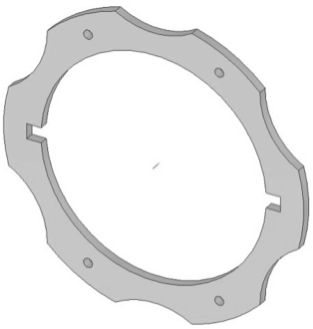

(b) 3-D view of a ring element of the anti-sloshing device.

Figure 1: 3-D detailed views of the anti-sloshing device.

2.2 Experimental set-up

During a flight, the rocket moves around its center of gravity and the oxidizer tank is submitted to vibrations evolving in a frequency range from 1 Hz to 10 Hz. A dedicated test bench has been designed to reproduce this range of solicitations and then characterize the efficiency of the anti-sloshing device proposed in the previous section. To be able to visualize the liquid behavior, a transparent cylindrical tank has been designed and realized from a Plexiglas tube. Its radius is $5.5 \cdot 10^{-2}$ m while its total length is $55.0 \cdot 10^{-2}$ m. The test campaign has been conducted using water because both its density ρ and its viscosity μ are close to that of typical liquid oxidizers such as N_2O. The anti-sloshing system has been

realized so that it can be easily placed and withdrawn from the transparent tube. Experimental measurements of the sloshing amplitudes can then be performed with and without the anti-sloshing device and using different initial filling levels of the tank.

To reproduce realistic excitation, a chariot moved by a link-crank system is periodically translated on a rail. Assuming that oxidizer tanks are mainly submitted to transverse oscillations, the system has been limited to horizontal excitation (i.e. orthogonal to the axis of the tank). Because of the acceleration, the liquid is forced against the walls while axial excitation is limited. The bench was fixed to a heavy table to reduce the energy losses caused by vibration. The rigidity of the system and the limitation of the friction are crucial to the precision of the measures. The sloshing test bench is shown in Figure 2.

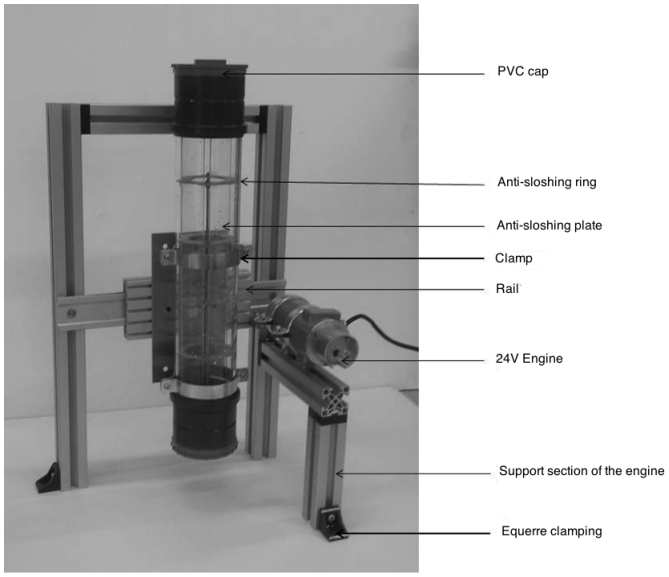

Figure 2: Direct visualization of the experimental test bench. The transparent tube including the anti-sloshing device is mounted.

2.3 Sloshing measurements

A precise instantaneous measurement of the overall sloshing of the liquid within the transparent tank is not straightforward. In the context of an incompressible liquid, the study can be reduced to the movement of the liquid-air interface. This free-surface motion is representative of the whole liquid movement. This interface is then tracked using a high resolution camera. The amplitude of the waves is estimated by image post-processing using the software *Latis Pro*.

Dodge and Kana [10] developed an experimental protocol to make such measurements. They propose to proceed as follows:

1. Start the transverse excitation of the liquid by starting the forced translation movement of the tank.
2. When the movement of the liquid is periodic, the forced translation is stopped.
3. The free liquid-air interface tracking starts once the forcing is stopped.

Following this methodology, the sloshing decay rate of the tracked movement characterizes the anti-sloshing device efficiency. In the present study, the Dodge and Kana procedure has been slightly modified and the measurements are performed while the forced translation motion of the tank is maintained. This approach seems to be more representative of what happens in real flight conditions. Therefore, the anti-sloshing device efficiency during forced translation motion is evaluated by comparing the wave amplitude whether the device is installed or not. The measurements are obtained following this protocol:

1. Start the transverse excitation of the liquid by starting the forced translation movement of the tank.
2. When the movement of the liquid is periodic, the free liquid-air interface movement acquisition starts.
3. When the measurements time window ends, acquisition is stopped.

4. The forced translation movement of the tank is stopped.

Experimental results are analyzed in the following section in order to quantify the efficiency of the anti-sloshing device.

2.3.1 Anti-sloshing device efficiency

Figure 3 shows the temporal evolution of the maximum liquid height along the tube. As expected, it can be seen that the maximum of amplitude seems to be higher when the tested device is not used. A global $1s$-periodicity can be found for both curves and is attributed to the first asymmetrical sloshing mode. The curve identified with squares clearly shows an envelope curve with a $3s$-periodicity. This envelope curve is attributed to the second rotational sloshing mode and is characterized here by a lower frequency. It is now proposed to conduct a spectral analysis in order to further investigate the effect of the anti-sloshing device on the liquid-air interface movement.

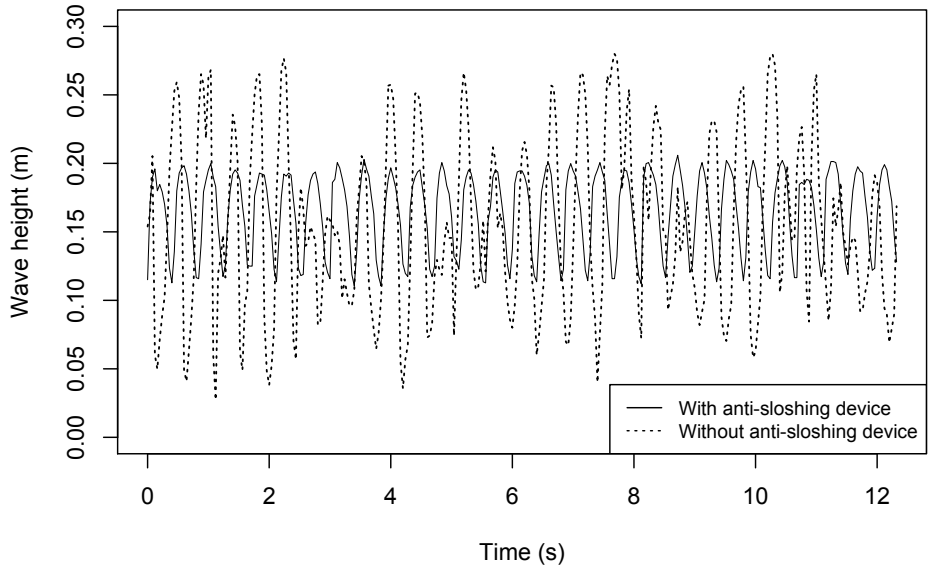

Figure 3: Temporal evolution of the maximum waves amplitude with and without anti-sloshing device for a transverse excitation at 2.2 Hz and liquid load of 3.77 kg.

Figure 4 shows the associated Fourier transforms of the two temporal signals plotted in Figure 3. The plotted case corresponds to a transverse excitation of 2.2 Hz. This forcing frequency also matches the main peak of the spectral decomposition. The surface under the curve is an estimation of the energy created by the movement of the fluid. In this work, the use of a spectral analysis allows both to identify the main frequencies of the fluid response and to compare the energy associated to each frequency (i.e. the area under a given frequency range). The comparison between the two measured cases can then be easily conducted.

Figure 4 clearly shows that using the anti-sloshing device greatly reduces the amplitude of the waves on the whole studied frequency range. The device acts as a large-band filter. Therefore, the energy contained in the curve obtained with the device is 3 times lower that in the curve without the device. The very high energy content at low frequencies, attributed to the second rotating sloshing mode, is completely damped when the anti-sloshing device is used. Higher frequencies, attributed to the third chaotic sloshing mode, show a wider amplitude distribution and are also significantly decreased.

The presented results confirm that the proposed anti-sloshing device limits the liquid movements for all the elementary sloshing modes. This device can be realized easily and can be adapted to any other tank geometry. The probability of a feeding interruption due to high sloshing modes significantly decreased and further work on injection process can now be performed.

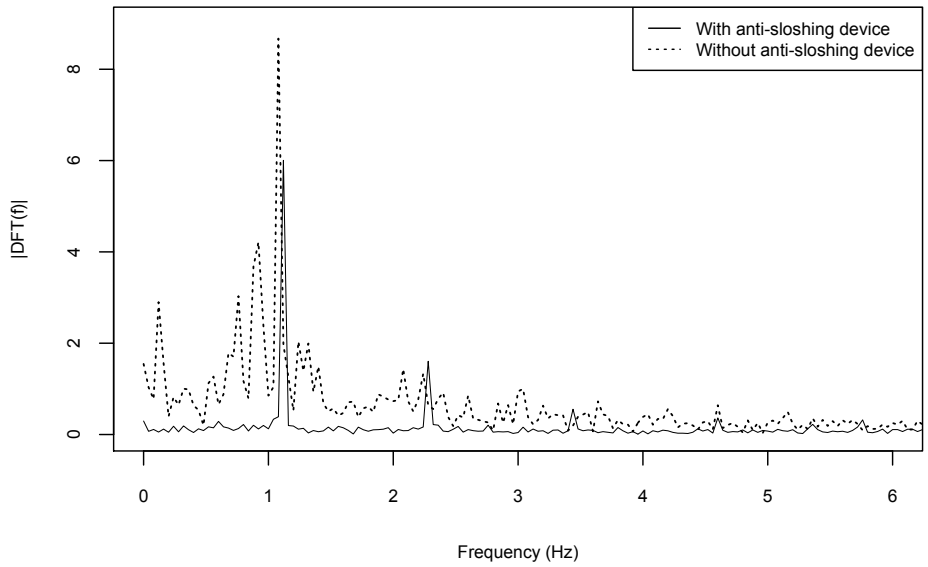

Figure 4: Fourier transforms of the amplitudes of the waves with and without anti-sloshing device for a transverse excitation at 2.2 Hz and liquid load of 3.77 kg.

3. Design of an injector for hybrid rocket engines

The injector is a key subsystem for the HRE since it controls the overall behavior of the motor in terms of fuel atomization and distribution, combustion efficiency and combustion stability. Combustion process in HRE mainly exhibits a non-premixed flame. This flame is controlled by the turbulent mixing of the oxidizer and the vaporized fuel. However, the mechanism of fuel melting resulting from the heat transfer from the flame front to the fuel surface is the limiting phenomena in term of characteristic time scales. One way to improve combustion efficiency is then to provide more chance for mixing by introducing strong chamber aerodynamics, increasing the heat transfer to the fuel layer and consequently the regression rate. Since the reaction between the oxidizer and the fuel takes place at gaseous state, it is also essential that the oxidizer enters the flame front in a fully vaporized state. The injector has to ensure a good atomization and allow a homogeneous oxidizer distribution along the combustion chamber.

Among the existing injector technologies, the axial injector is interesting for its simple design and its ability to produce stable combustion with very little pressure oscillation [1] due to a hot gas recirculation zone inside the pre-chamber that heats-up the oxidizer and accelerate the vaporization process. To enhance mixing inside the combustion chamber, swirl injectors have been widely used because of their geometric simplicity and very efficient atomization. The liquid oxidizer enters a vortex chamber through tangential inlets inducing a high angular velocity. The rotating motion forces the liquid to form a thin sheet and to exit the vortex chamber with a conical shape. As the cone expands, the liquid sheet becomes thinner and is prone to instabilities, leading to the liquid atomization. Lee *et al.* [12] have shown that the swirling injection results increase by 50% the regression rate for a given combustion chamber geometry leading to a 30% increase in specific impulse (ISP) compared to non-swirling conditions. ISP is defined as ISP = $\frac{F}{\dot{m}_{tot} \cdot g}$ where g is the acceleration at the Earth's surface, $\dot{m}_{tot}$ is the total mass flow rate and F is the thrust obtained from the HRE. However, Lee *et al.* [11] noticed that the regression rate increase is effective only in regions close to the injector and not uniform across the combustion chamber.

3.1 Investigated injector

On the one hand, axial injectors provide a stable but poorly efficient combustion due to the bad quality of the atomization process. On the other hand, swirl injection improves combustion efficiency but has effects limited to the first half of the fuel grain. This technology also tends to produce high pressure oscillation that may reduce the overall performance as shown in [13]. Based on the previous qualitative considerations, a new injector has been designed. It is composed

of an axial orifice surrounded by a swirl vortex chamber. The aim of this injector is to provide a homogeneous oxidizer distribution along the combustion chamber and to combine the advantage of both axial and swirl injectors (i.e. stable combustion and good atomization properties respectively). By introducing a swirl component in the injector flow, it is expected that better atomization and mixing will improve the overall engine performance. Dimensions of the prototype were based on the study conducted in [14] and are shown in Fig. 5a.

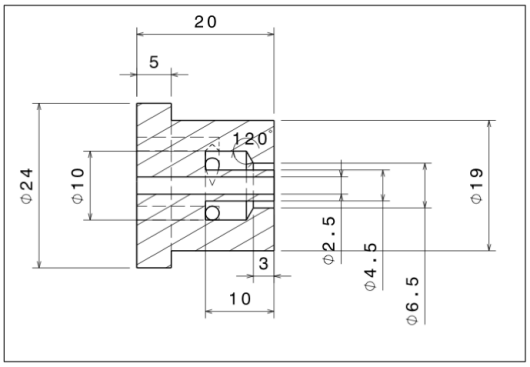

(a) 2-D view of the axi-swirl oxidizer injector.

(b) Direct visualization of the axi-swirl oxidizer injector.

Figure 5: 2-D cut and direct visualization of the axi-swirl oxidizer injector.

3.2 Isothermal characterization

To ensure balanced mass flow rates through each injection channel, a 3-D isothermal steady RANS simulation was performed on this prototype using a commercial software [15]. The turbulent model SST $k-\omega$ (Shear Stress Transport) was used to account for the pressure drop along the injector wall. The fluid used is liquid water. A particular care has been paid to mesh refinement near the injector walls (y^+ parameter has been found between 1 and 5 in these regions). The ratio $\alpha = \frac{\dot{m}_{ax}}{\dot{m}_{ax}+\dot{m}_{sw}}$ between the axial mass flow component $\dot{m}_{ax}$ and the total mass flow rate $\dot{m}_{ax} + \dot{m}_{sw}$ was obtained for pressure drops from 3 to 50 bars. Total simulated mass flow rate $\dot{m}_{ax}+\dot{m}_{sw}$ are plotted in Fig. 6a while corresponding values of α are shown in Fig. 6b. For this range of pressure, α is found relatively constant and close to 40%.

Considering the satisfying numerical results, the prototype was realized and tested using a cold water flow to confirm the numerical approach. Each injection channel was roughed separately from a brass alloy and then welded together. The axial and tangential inlets were bored and the tangential inlets were partially filled to form the elbow shape. The whole piece was lathed to adopt the proper dimensions and is shown in Fig. 5b. Two maintaining pieces shown in Fig 7 were machined to support the injector and facilitate future cold flow and reacting tests.

The cold flow test on this prototype was performed to measure the water total and axial mass flow rates for a pressure drop going from 1 to 4 bars. Water flowed from a 5 bar supply through a manometer into the injector and was received into a tank. The mass of water and the duration of the experiment allowed to find an average experimental mass flow rate. Experimental results are compared to the numerical results in Fig. 6. Simulated total mass flow rate $\dot{m}_{ax} + \dot{m}_{sw}$ and balance ratio α values show a good agreement with the experimental data.

3.3 Reacting characterization

Reacting tests were performed on this new injector to compare the specific impulse (ISP) gain over a simple axial injector. The HRE test bench consisted of a hybrid motor, from the rocketry manufacturer *Sky Ripper System*, modified to allow ground testing with different injectors. This HRE uses N_2O as an oxidizer and Acrylonitrile Butadiene Styrene (ABS) as a fuel. The original HRE is shown in Fig.8a while the modified HRE is displayed in Fig. 8b. Modifications consisted on replacing the original injection system by a proper device capable of operating the investigated injector as well as the reference axial injector. The initial plastic filling tube was withdrawn and replaced by an external filling system along with an electric valve to start injection of the oxidizer into the combustion chamber. The modified filling system is detailed in Fig. 8c.

The rocket thrust F is measured using a load cell. The fuel consumption m_{fuel} is estimated from the grain mass defect after firing. The consumed oxidizer mass v is obtained using a 10 kg counterbalance weight, shown in Fig. 9, to

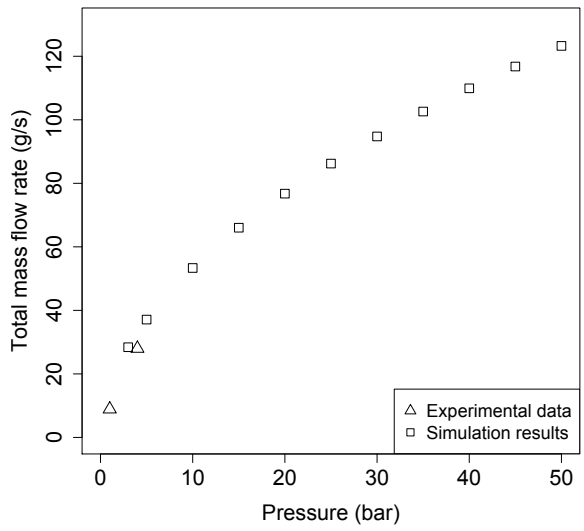

(a) Total mass flow rate $\dot{m}_{ax} + \dot{m}_{sw}$ function of the inlet pressure drop.

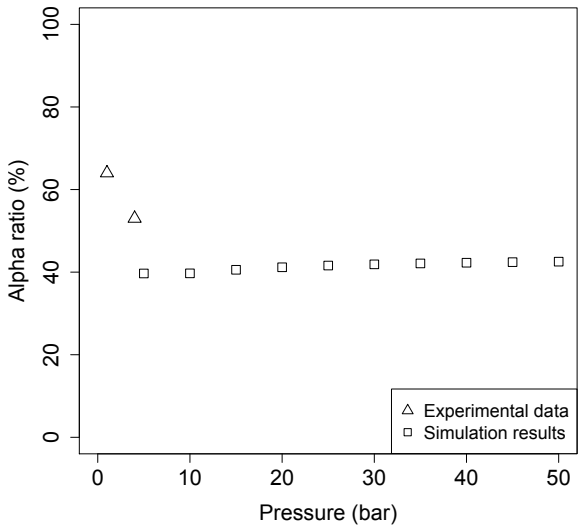

(b) Axial-to-total mass flow rates $\alpha = \frac{\dot{m}_{ax}}{\dot{m}_{ax}+\dot{m}_{sw}}$ ratio function of the inlet pressure drop.

Figure 6: Axial-to-total mass flow rates ratio α and total mass flow rates $\dot{m}_{ax} + \dot{m}_{sw}$ function of the inlet pressure.

Figure 7: Maintaining device to hold the injector

press the thrust collector against the load cell. It is then possible to obtain the difference between the tank weight at the beginning and at the end of the filling process. This measured mass of oxidizer m_{ox} is considered as fully consumed.

Reacting tests were performed using the following procedure :

1. The filling valve is opened which starts the filling of the rocket tank.
2. The filling valve is closed when the N_2O vent is noticeably leaking.
3. A pyrotechnic device preinstalled in the combustion chamber is lit and the solenoid valve is simultaneously opened to ignite the HRE.
4. The solenoid valve is closed after approximately 8 s to end the test.

3.4 Results and discussion

Two reacting tests were performed. The first test was carried out with the reference axial injector, and the new injector was used for the second test. The experimental ISP estimated as $\text{ISP}_{exp} = \frac{F\Delta t}{(m_{ox}+m_{fuel})g}$ was found for the first test, but not for the second test because of an identified malfunction in the acquisition process. To allow comparison, the theoretical ISP for both tests was found using ideal performance data of the N_2O - ABS couple detailed in Fig. 10. Results are presented in Tab. 1. The most important point is that an overall ISP improvement of 11 s is found for the experimented combustion chamber geometry.

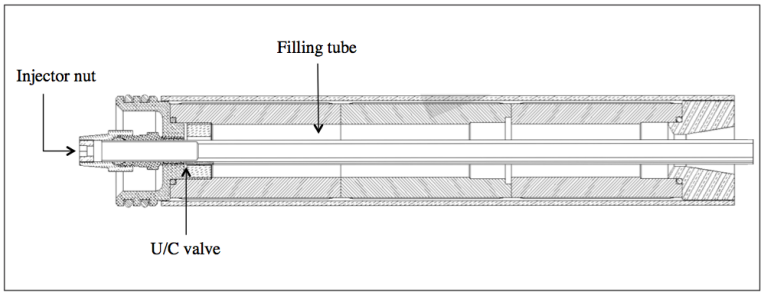

(a) 2-D view of the original HRE

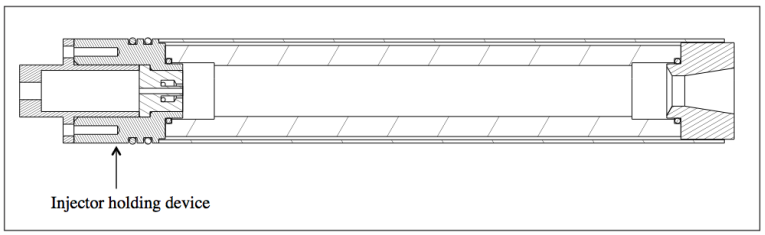

(b) 2-D view of the modified HRE

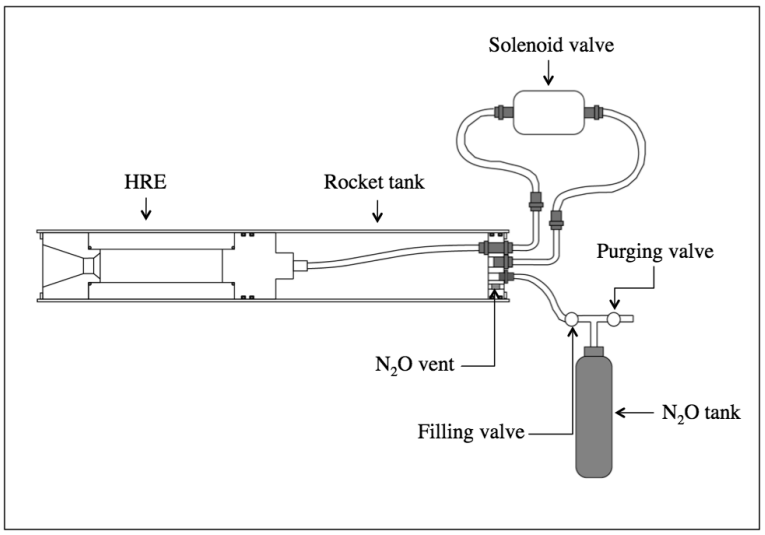

(c) Diagram of the modified HRE filling System

Figure 8: Injector test bench for the reacting characterization.

The new injector performs better than a reference axial injector. However, it is not clear whether it is the combination of swirl and axial or just the new added swirl component that provided this satisfying result. In the latter case, it would have been even higher with pure swirl injection. Further work is then needed to investigate a possible optimum of the α ratio in terms of combustion efficiency.

4. Conclusion

This study, conducted by a first year engineering student group, aimed to add a contribution to the Hybrid Rocket research field by proposing simple HRE subsystems and testing them. An anti-sloshing system has first been proposed. The use of a simple combination of existing systems allowed to design a light and efficient anti-sloshing device. A slightly different characterisation methodology was used compared to literature. Both the ability to limit global fluid sloshing and to damp the three sloshing modes were investigated. An original injector prototype was then presented. The proposed design is based on both literature review and qualitative analysis. A characterization of the injector has been conducted through both an isothermal and a reacting test campaigns. The axi-swirl technology is found to perform better than the reference axial injection. Further investigations are needed to characterize the injector properties in terms of combustion stability and mass flow repartition through the injection channels of the HRE combustion chamber.

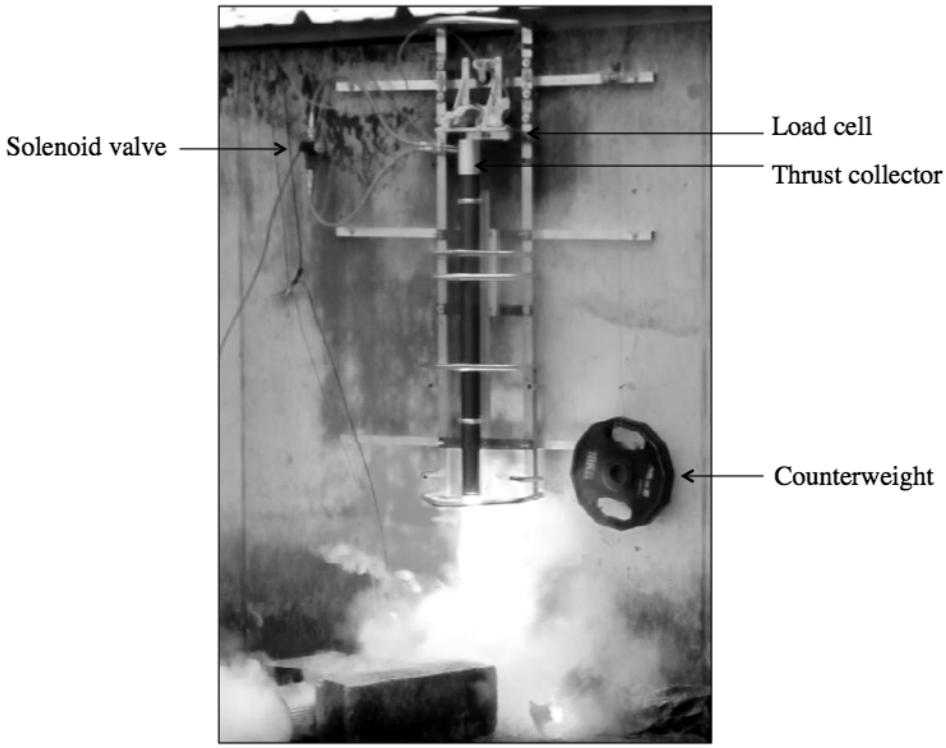

Figure 9: Direct visualization of the reacting HRE test bench during a firing test.

Table 1: Summary of results obtained from the reacting test campaign.

	Thrust	Duration	Fuel mass consumption	Oxydizer mass consumption	O/F ratio	Experimental ISP	Theoretical ISP
Axial injector	310 N	2.5 s	23.8 g	400 g	16.8	186.4 s	213 s
Axi-swirl injector	⊘	⊘	29.9 g	400 g	13.4	⊘	224 s

References

[1] Sutton, G.P. and O. Biblarz. 2001. Rocket Propulsion Elements, 7^{th} edition. John Wiley & Sons.

[2] Greinear, B. and R.A. Frederick. 1993. Hybrid Rocket Instability. In: 29^{th} *AIAA/SAE/ASME/ASEE Joint Propulsion Conference & Exhibit*.

[3] Carmicino, C. and A. Russo Sorge. 2006. The Effects of Oxidizer Injector Design on Hybrid Rockets Combustion Stability . In: 42^{th} *AIAA/SAE/ASME/ASEE Joint Propulsion Conference & Exhibit*.

[4] Royon-Lebeaud, A. 2005. Liquid sloshing in cylindrical reservoirs subjected to an harmonic oscillation: non-linear wave regimes and breaking. PhD Thesis. Grenoble: Université Joseph Fourier.

[5] Abramson, H.N. 1966. The Dynamic Behavior of Liquids in Moving Containers. NASA SP-106.

[6] Carmicino, C. and A. Russo Sorge. 2005. Performance comparison between two different injector configurations in a hybrid rocket. In: *European Conference for Aeronautics and Space Sciences (EUCASS)*.

[7] Fu, Q., L. Yang and X. Wang. 2010. Theoretical and experimental study of the dynamics of a liquid swirl injector. *Journal of Propulsion and Power* 26.

[8] Fu, Q., L. Yang, Y. Qu and B. Gu. 2011. Geometrical effects on the fluid dynamics of an open-end swirl injector. *Journal of Propulsion and Power* 27.

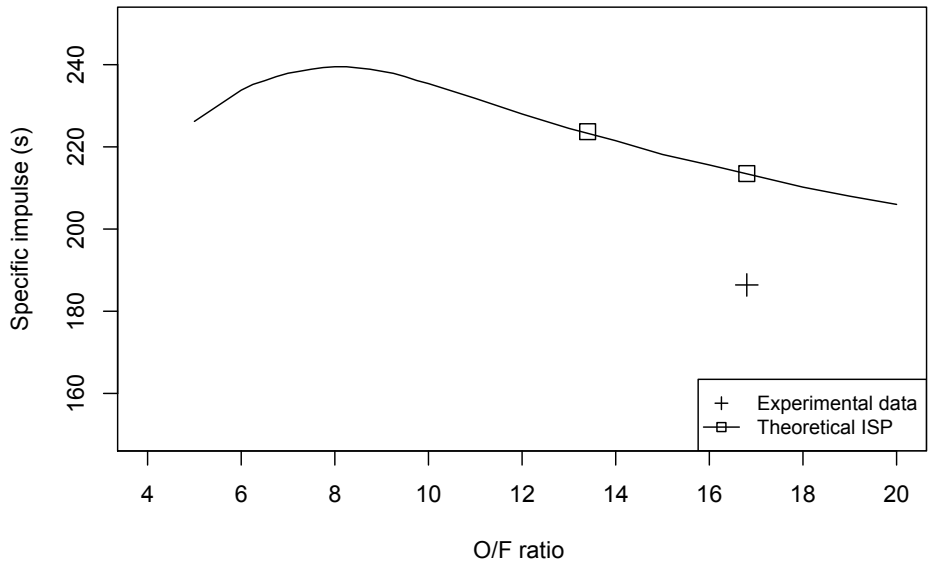

Figure 10: Theoretical ISP function of the ratio oxidiser to fuel mass flow rates. The solid line corresponds to the N_2O/ABS couple. □ denotes the theoretical values of ISP associated to both axial and axi-radial injectors test campaigns. + denotes the measured ISP values.

[9] Hamid, A.H., R. Atan. 2009. Spray characteristics of a jet swirl nozzles for thrust chamber injectors. *Aerospace Science and Technology* 13.

[10] Dodge, F.T. and D.D. Kana. 1966. Moment of inertia and damping of liquids in baffled cylindrical tanks. *Journal of Spacecraft and Rockets* 3, pp. 153-155.

[11] Lee, C., Y. Na, J.W. Lee, and Y.H. Byun. 2007. Effect of induced swirl flow on regression rate of hybrid rocket fuel by helical grain configuration. *Aerospace Science and Technology* 11.

[12] Lee, T.S. and A. Potapkin. 2002. The performance of a hybrid rocket with swirling gox injection. Technical report.

[13] Haeseler, D. . 2003. Injector issues with different propellant combinations. in; 5^{th} *International Symposium on Liquid Space Propulsion*, Chattanooga, TN, USA.

[14] Park, H. and S. Heister. 2006. Nonlinear simulation of free surfaces and atomization in pressure swirl atomizers. *Physics of Fluids* 18.

[15] ANSYS® Fluent. 2009. Release 12.0.